Metal-Insulator-Metal Surface Plasmon Polariton Waveguide Filters with Cascaded Transverse Cavities

Lorena O. Diniz, Frederico D. Nunes, *Member, OSA*, Euclydes Marega Jr., John Weiner, *Member, OSA*, and Ben-Hur V. Borges, *Member, IEEE, OSA*

***Abstract*— In this work we propose a new approach for the design of resonant structures aiming at wavelength filtering applications. The structure consists of a subwavelength metal-insulator-metal (MIM) waveguide presenting cascaded cavities transversely arranged in the midpoint between the input and output ports. An extra degree of freedom added to this design consists in tilting the cavities around their midpoints which, besides effectively increasing the quality factor of the cavity, helps extending its range of applications by tuning multiple wavelengths.**

***Index Terms*—Cavity resonator filter, surface plasmon polariton, SPP, waveguides.**

I. Introduction

THE rapid development of the field of plasmonics observed in the past few years has paved the way for the development of a myriad of devices capable, for example, of guiding, coupling, or filtering wavelengths at scales below Abbe's diffraction limit. This remarkable ability has rendered surface plasmon polariton (SPP) based devices particularly important for telecom and sensing applications, as it allows miniaturizations at unprecedented scales. Yet, SPP based devices can be as simple as the combination of two semi-infinite materials, i.e., a metal and an insulator. At optical wavelengths, such an interface can guide transverse magnetic (TM) surface waves [1], which is possible due to the coupling of the electromagnetic field to the conduction electrons in the metal. The disadvantage of this effect is that ohmic losses can reduce SPP propagation to only a few tens of microns for noble metals in the visible or near-infrared wavelengths [2]. Therefore, the choice of the waveguiding scheme plays an important role on the overall performance of any SPP based device.

Several SPP waveguiding schemes have been successfully proposed in the literature, such as metal films of finite width [3-5], dielectric loaded directional couplers [6], dielectric stripes on gold [2, 7], straight waveguides coupled to lateral stubs [8-10], insulator-metal-insulator and metal-insulator-metal structures [11]. Metal-insulator-metal (MIM) structures in particular, have become of great interest due to their ability to provide superior field confinement (or localization) when compared to the other schemes mentioned above. This better field localization is obtained at the expense of a higher propagation loss (reduced propagation distance). It should be noticed that despite the higher propagation loss, MIM based SPP structures have been successfully employed in wavelength filtering applications (the focus of this work), where high quality factors are desired. Several approaches have been investigated in the literature for this purpose, such as teeth-shaped structures [12-17], gap based filters [18-20], and ring/disk based resonators [21].

As is well known, an important aspect of wavelength filtering devices is the ability to provide high wavelength selectivity. This requires a high quality factor Q ($Q = \lambda_0 / \Delta\lambda$, where λ_0 is the peak wavelength and $\Delta\lambda$ is the half width of the peak). However, this parameter can be substantially reduced by the ohmic losses of SPP waveguides, thereby sacrificing selectivity. In [19], for example, the quality factor Q is as high as 50, while in [20] it is less than 25. Other configurations, such as plasmonic ring/disk resonators have also been suggested for wavelength selection purposes, resulting in a quality factor Q = 30 [21].

In this context, the present work explores a novel approach for the design of resonant structures based on cascaded cavities aiming at wavelength filtering applications. An extra degree of freedom included in the analysis consists in tilting the cavities around their central points. Results show this approach can produce quality factors in excess of 500, which is extremely high for MIM-based structures. Moreover, we show that tilting the cavities not only helps to improve the quality factor, but also allows one to simultaneously select multiple wavelengths (this effect is not observed for vertical single cavities).

Manuscript received September 5, 2010. This work was supported in part by the Brazilian agencies FAPESP, CAPES and CNPq.

L. O. Diniz and B.-H. V. Borges are with the University of São Paulo, São Carlos School of Engineering, Electrical Engineering Department, Av. Trabalhador São-Carlense, 400, 13566-590, São Carlos, SP, Brazil (corresponding author +55-16-3373-8132; fax:+55-16-3373-9372; e-mail: benhur@sc.usp.br).

F. D. Nunes, is with the Federal University of Pernambuco, Electrical Engineering Dept., Recife, PE, Brazil.

E. Marega Jr. is with the University of São Paulo, Physics Institute, São Carlos, SP, Brazil.

J. Weiner is with the Center for Nanoscale Science and Technology, National Institute for Standards and Technology, 100 Bureau Drive, Mail stop 6203, Gaithersburg, MD 20899, United States.

Digital Object Identifier inserted by IEEE

II. Mathematical Background

The top view of the proposed cascaded filter design is schematically shown in Fig. 1(a). In this approach the possibility of tilting the cavities (dashed lines) is also explored. The idea is to investigate how the tilting of the cavity affects the overall performance of the device. In this section we describe the simplified mathematical model that physically describes the resonance condition for a single cavity [22]. This model is based on the scattering matrix theory, also adopted in the design of tooth shaped waveguide filters [12], expanded here to a four port structure. We have observed that the resonant frequency of cascaded cavities can also be accurately predicted with this simplified single cavity analysis. Therefore, and with the help of Fig. 1(b), the transmittance from Port 1 to Port 2 is obtained as follows,

$$\begin{bmatrix} E_1^{out} \\ E_2^{out} \\ E_3^{out} \\ E_4^{out} \end{bmatrix} = S \begin{bmatrix} E_1^{in} \\ E_2^{in} \\ E_3^{in} \\ E_4^{in} \end{bmatrix}, \text{ with } S = \begin{bmatrix} r_1 & t_1 & s_3 & s_3 \\ t_1 & r_1 & s_3 & s_3 \\ s_1 & s_1 & r_3 & r_3 \\ s_1 & s_1 & r_3 & r_3 \end{bmatrix}.$$

In the above equations, r_i, t_i, and s_i (i = 1,2,3,4) are, respectively, the reflection, transmission, and splitting coefficients of the incident wave from Port i. $E_i^{in,out}$ refers to the incident/output field at the specified port. Expanding the above system and assuming $E_2^{in} = 0$, one obtains,

$$E_2^{out} = t_1 E_1^{in} + s_3 E_3^{in} + s_3 E_4^{in}, \text{ and} \quad (1)$$

$$E_{3,4}^{in} = \frac{s_1 E_1^{in}}{1 - r_3 e^{i\theta(\lambda)}} e^{i\theta(\lambda)}. \quad (2)$$

Substituting (2) into (1), yields

$$E_2^{out} = t_1 E_1^{in} + \frac{2 s_1 s_3 E_1^{in}}{1 - r_3 e^{i\theta(\lambda)}} e^{i\theta(\lambda)}.$$

In the above equations, the phase delay $\theta(\lambda)$ is given by $\theta(\lambda) = (4\pi/\lambda) n_{eff} h_1 + \Delta\varphi(\lambda)$, where $n_{eff} = \beta / k_0$ (β is the propagation constant, and $k_0 = 2\pi/\lambda_0$), and $\Delta\varphi(\lambda)$ is a phase shift at the air/silver interface. Finally, the transmittance from Port 1 to 2, can be obtained as

$$T = \left| \frac{E_2^{out}}{E_1^{in}} \right|^2 = \left| t_1 + \frac{2 s_1 s_3}{1 - r_3 e^{i\theta(\lambda)}} e^{i\theta(\lambda)} \right|^2. \quad (3)$$

From (3) one can obtain the wavelength for maximum transmission, which is given by

$$\lambda_m = \frac{4 n_{eff} h_1}{(2m+1) + \frac{\Delta\varphi}{\pi}}, \quad (4)$$

where the effective index n_{eff} is an implicit function of w_1. As will be discussed in the next section, the width w_1 influences only weakly the position of the through wavelength (and also Q).

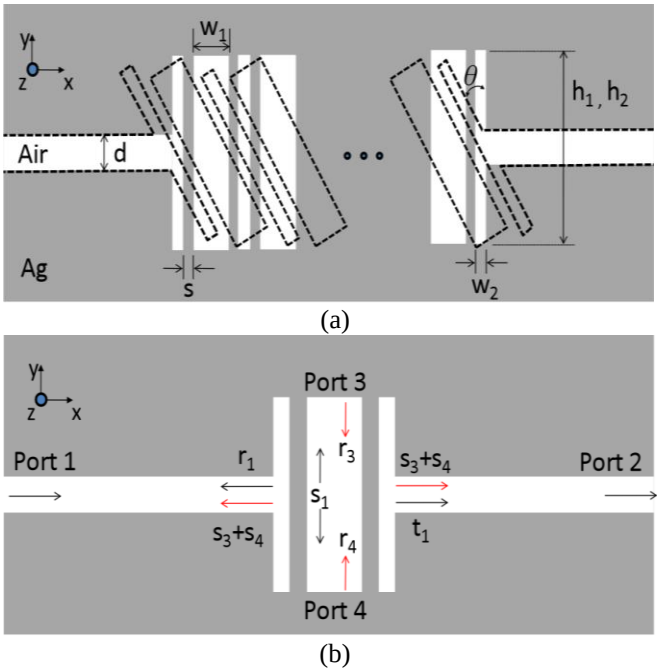

Fig. 1: (a) Top view of the slit-based cascaded filter; h_1 and h_2 are the heights of the central cavity and lateral arms (stubs), respectively. The depth of the slit is assumed as p (not shown in this figure). (b) Schematic diagram utilized with the Scattering Matrix Formalism for a four-port single cavity structure.

III. Numerical Results

The metal used in the simulations is silver, whose permittivity is defined here via polynomial fitting of the experimental data from Johnson and Christy [23]. All simulations discussed in this section where carried out with *COMSOL Multiphysics*[1] for TM polarized waves [24]. The waveguide width d is kept constant in all simulations (d = 150 nm), and the operating wavelength is λ_m = 1000 nm. The cavity height, h_1, is then obtained from (4) assuming m = 3 and $\Delta\varphi(\lambda) = 0$, without loss of generality. The effective index in that equation is obtained via two-dimensional simulation of the central cavity cross-section assuming a slit width w_1 = 240 nm and a slit depth p = 400 nm. This slit depth guarantees a good compromise between loss and field confinement. A thorough investigation of MIM structures in terms of mode effective index, propagation distance, and mode confinement

[1] The identification of the *COMSOL Multiphysics* software package is not intended to imply recommendation or endorsement by the National Institute of Standards and Technology, nor is it intended to imply that this product is necessarily the best available for the purpose.

is beyond the scope of this paper, but for the resonant wavelength of 1000 nm these parameters are, respectively, n_{eff} = 1.013306 - *i* 3.591894×10^{-4}, 221.55 μm, and 37.04, with the last two obtained according to [25]. The cavity parameters *s*, h_2, and θ, as well as the number of cascaded cavities, will be individually analyzed next. By virtue of the large number of variables to be optimized in the cascaded cavities structure in Fig. 1(a), we decided first to design a single cavity device and, afterwards, replicate the obtained parameters to as many consecutive cavities as desired. We found that this procedure does not significantly affect the operating point of the cascaded structure. The single cavity design was explored in our previous publication in [22], and is now summarized here for the sake of convenience.

First, the results will be obtained for a cavity tilting angle θ = 0°. An interesting aspect of this structure is the lateral arms on each side of the central cavity. These arms (or stubs) perform an important role in the energy coupling to the cavities, with a direct influence both on the cavity *Q* and on the insertion loss. The frequency response for a single cavity for three different arm heights, i.e., $h_2 = h_1$ (circles), $h_2 = 3h_1/7$ (squares), and $h_2 = d$ (triangles) is shown in Fig. 2(a). We have fixed the following parameters: $s = 35$ nm, $w_1 = 240$ nm, and $w_2 = 50$ nm. When the arms are not present ($h_2 = d$) the best *Q* is obtained (*Q* = 450). In this case, the coupling efficiency to the central cavity is sacrificed, resulting in an insertion loss of -9.81 dB. For $h_2 = h_1$ ($h_2 = 3h_1/7$), the cavity *Q* and insertion loss are, respectively, 63 (170) and -0.99 dB (-3.07 dB). In this case we have chosen $h_2 = 3h_1/7 = 743$ nm as a good compromise between selectivity and insertion loss. As will be shown later on, this corresponds to a total stub height h_2 that is close to λ_{SPP} ($\lambda_{SPP} = \lambda_m / n_{eff}$). By doing so, the wave pattern inside the stub closely matches the wave pattern inside the central cavity, therefore improving energy coupling between them.

Next, we analyze the influence of the cavity mirrors' thickness *s* on the frequency response, Fig. 2(b). All remaining geometrical parameters remain the same as above. As one would expect, only one resonant peak is obtained for this case. In addition, as *s* increases so does the mirrors reflectivity and, consequently, the cavity *Q* (at the expense of a lower transmission). Therefore, $s = 35$ nm is an adequate compromise between wavelength selectivity and transmission loss. Now that all pertinent geometrical parameters for the single cavity are defined, we simulate the influence of multiple cavities and tilting angle on the filter's overall frequency response. The simulated results for up to four cascaded cavities are shown in Figs. 3(a)-(d), for single, two, three, and four cavities, respectively. The limiting case is the single cavity (a) for θ = 0° (squares), adopted here as a reference condition for the sake of comparison. Observe that the resonant peak is blue-shifted by approximately 30 nm from the desired operating wavelength predicted with (4) (same is true for all other tilting angles). We believe this difference is caused by the assumption of ideal metal (perfect conductor) in the analytical model and real metal in the numerical simulations.

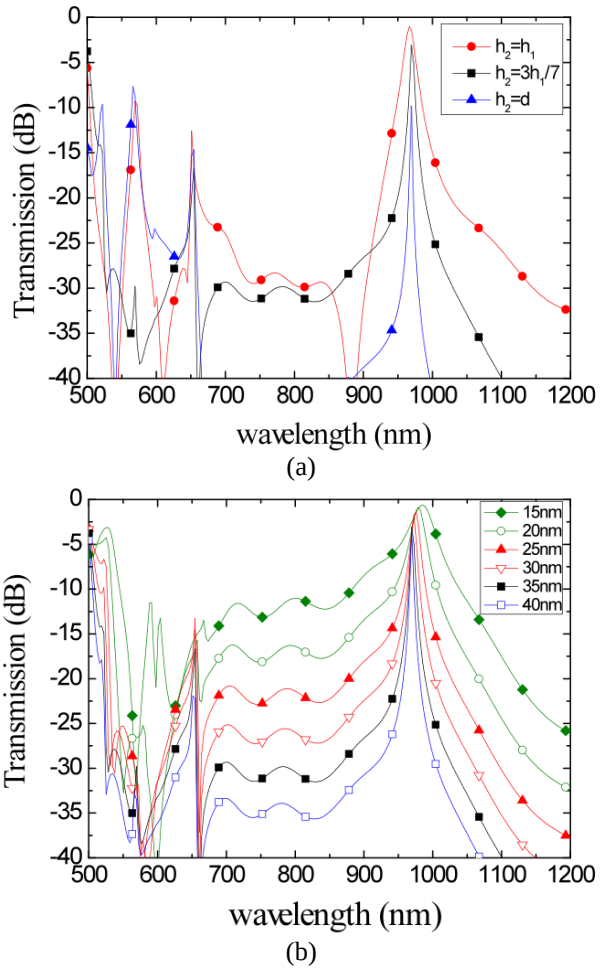

Fig. 2: Frequency response for a single cavity with the height of the coupling arms h_2 (a) and mirrors' thickness *s* (in nm) (b) as parameters. Each curve has 500 wavelength points. We used only a few symbols on each curve just to ease its readability.

Now, as the tilting angle increases, additional resonant peaks appear. It is important to remember at this point that larger tilting angles effectively increases mirror reflectivities, with a corresponding increase in *Q*. Therefore, one could argue that the additional resonant peaks should be attributed to this effect. But this is not true as can be seen in Fig. 2(b). No additional resonant peak is observed in that figure for thicker mirrors. Therefore, the tilting angle does plays an important role in the device's overall performance. This influence will be addressed later on.

When two or more cascaded cavities are considered the overall frequency response of the structure changes dramatically, see Figs. 3 (b)-(d) for 2, 3 and 4 cavities, respectively. All resonant peaks observed with the single cavity case (a) are still present here, but this time with a much higher *Q*-factor (as well as transmission loss). This is expected since the composite response of the cascaded structure is the product of individual cavities responses (if the cavities do not interact). Table 1 summarizes the influence of the tilting angle on the *Q*-factor and transmission loss for 1, 2, 3, and 4

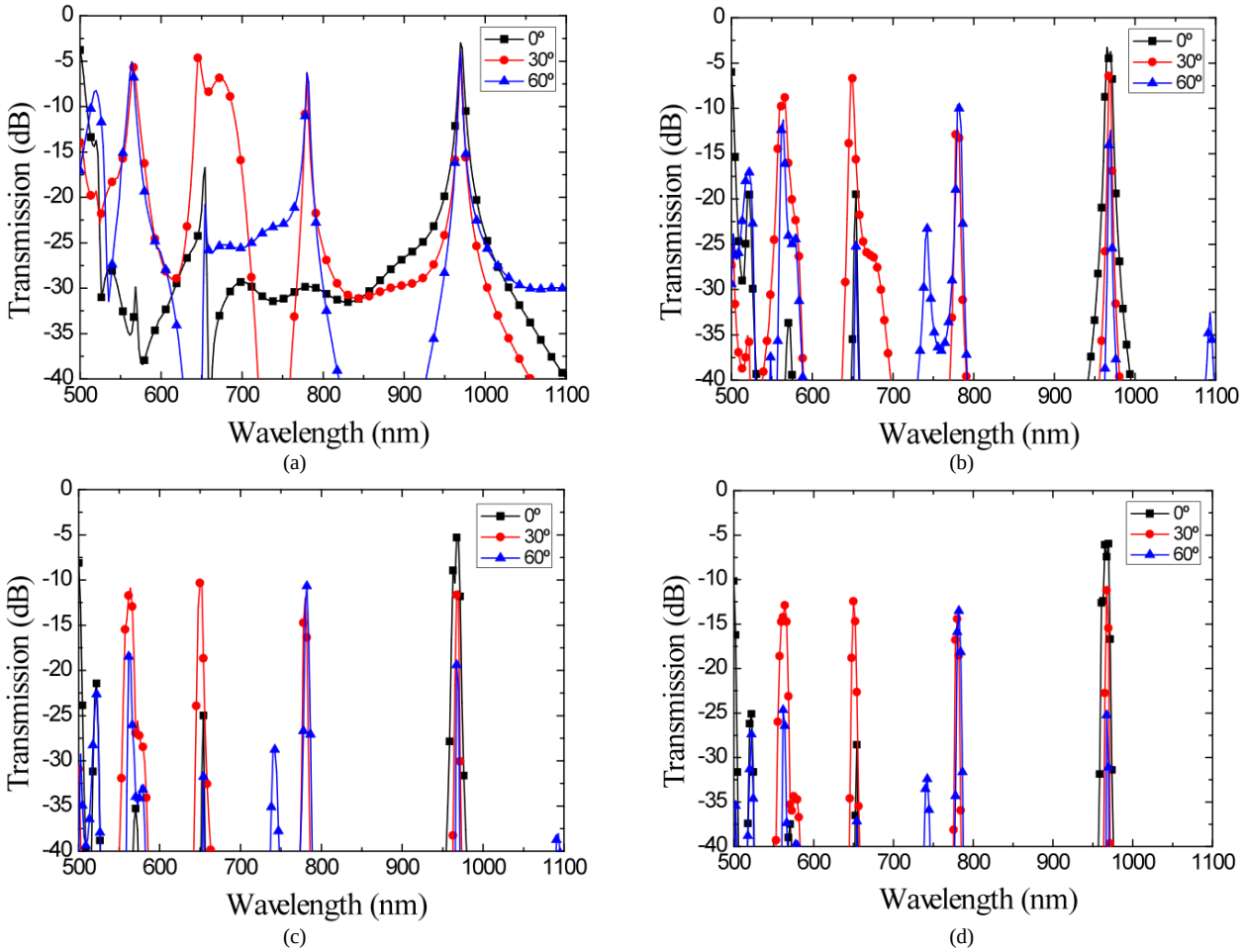

Figure 3: Frequency response with the tilting angle as a parameter. (a) single cavity, (b) two cavities, (c) three cavities, (d) four cavities. Each curve has 500 wavelength points. We used only a few symbols on each curve just to ease its readability.

TABLE I
Q-FACTOR AND TRANSMISSION LOSS IN TERMS OF THE TILTING ANGLE FOR 1, 2, 3 AND 4 CASCADED CAVITIES. WE HAVE HIGHLIGHTED THE CASES THAT COULD BE SUCCESSFULLY EMPLOYED IN WAVELENGTH SELECTIVE APPLICATIONS

Angle (deg.)	Single cavity		Two cavities		Three cavities		Four cavities	
	Q	Loss (dB)	Q	Loss (dB)	Q	Loss (dB)	Q	Loss (dB)
0	**170**	**-2.5**	**180**	**-3.27**	**210**	**-4.5**	**214**	**-5.6**
30	**250**	**-3.8**	**291**	**-5.37**	**335**	**-9.17**	350	-11.04
35	**317**	**-4.77**	**480**	**-8.5**	525	-15.0	654	-19.46
40	**443**	**-6.8**	885	-25.73	1075	-42.75	1327	-60.05
45	388	-12.46	560	-17.32	655	-19.85	692	-25.34
50	550	-47.56	600	-52.68	654	-54.26	792	-57.87
55	365	-11.58	537	-17.52	645	-20.48	684	-23.3
60	**255**	**-4.3**	**543**	**-8.7**	618	-14.3	752	-19.11

cascaded cavities. We have highlighted some cases we believe could be successfully applied to wavelength selective applications. We have also set the upper transmission loss limit to 11 dB (in absolute value) since this loss magnitude is not uncommon for slit-based structures [19]. A quick look at this Table also shows that a good compromise between wavelength selectivity and transmission loss can be a two cascaded cavity structure tilted by 60°, resulting in a *Q* and transmission loss of 543 and -8.7 dB, respectively. The *Q*-factor and transmission losses as a function of the tilting angle is plotted in Figs. 4(a)-(b), respectively. This figure helps visualize the role played by the tilting angle on the filter response. For a filter with two or more cavities one can see a dramatic response for θ = 40° and 50°. At these specific angles, not only the field intensity becomes even more intense (by a factor of 3), but also the reflectivity of the filter back to

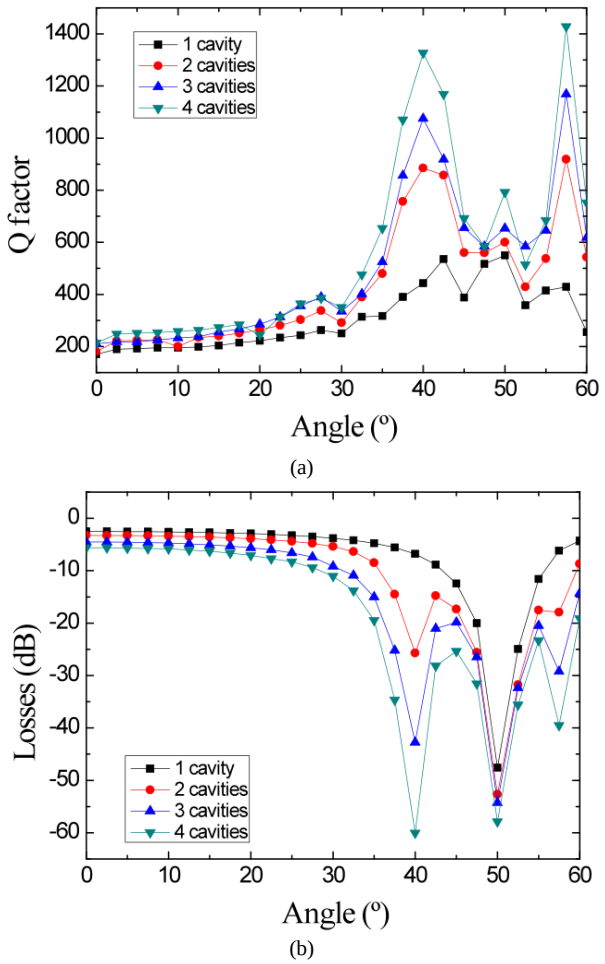

Fig. 4: Influence of the tilting angle on the *Q*-factor and transmission losses with the number of cascaded cavities as a parameter. The lines connecting the points are just to guide the eye.

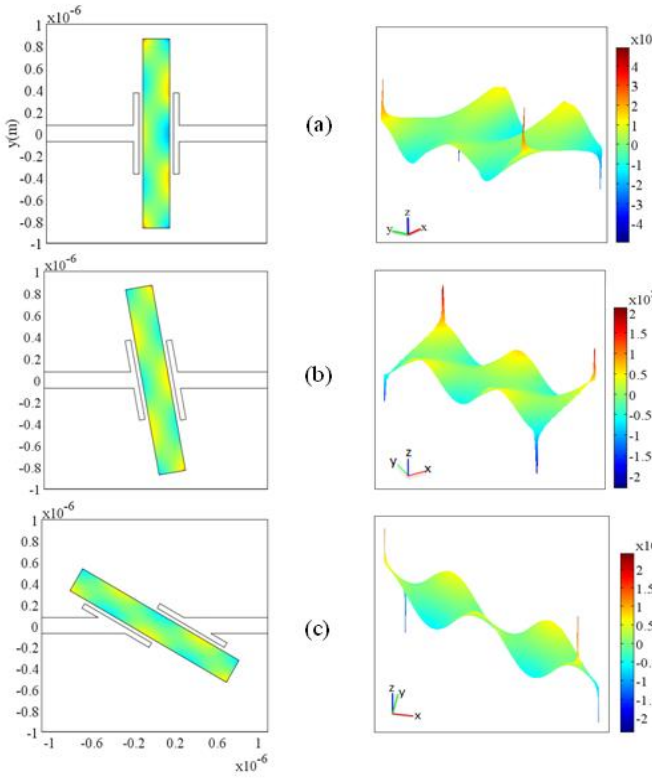

Fig. 5: Field distribution for the real part of the electric field component normal to the short axis of the cavity, $E_S=E_y\cos(\theta)-E_x\sin(\theta)$, for different tilting angles: (a) 0°, (b) 10°, and (c) 60°, taken at resonance. For the sake of clarity, only the field inside the cavity is shown. The field distributions in the right column show the oscillating dipoles (sharp peaks) at each corner of the cavity.

Port 1 (resulting in a much lower transmission). This increased field localization in the central cavity contributes to the extremely high wavelength selectivity observed for these particular angles. The non-monotonous behavior of the loss and Q-factor with tilting angle shows that the latter not only changes the optical path length inside the cavity (helping other wavelengths to satisfy the resonant condition) but also how the field interacts with metal. It is important mentioning at this point that the *Q*-factors obtained for the single cavity filter is far superior than those obtained with other slit-based structures [19-21].

To better illustrate the role played by the tilting angle on the overall response of the cavity we present in Figs. 5(a)-(c) the two-dimensional profiles of the real part of the electric field component normal to the short axis of the cavity for different tilting angles, i.e., 0°, 10°, and 60°, respectively. This component is chosen since it provides information regarding the oscillating charge distribution created on the edges of the cavity, and is obtained as follows: $E_S = E_y\cos(\theta) - E_x\sin(\theta)$. Similarly, the expression for the component normal to the long axis is defined as $E_L = E_y\sin(\theta) + E_x\cos(\theta)$. For the sake of clarity, only the field inside the cavity is shown. Observe that the electric field clearly shows the presence of sharp peaks at the four corners of the central cavity as a result of the accumulation of oscillating electrical charge at these particular locations. At 0° the oscillating charges (dipoles) on the left(right) corners have same sign and about the same intensity, but opposite signs with respect to the charges on the right(left) corners. The SPP mode launched at this angle establishes a standing wave along the short length of the cavity (which is about $\lambda_{SPP}/4$), and therefore it is referred here as a transverse SPP mode. At larger angles the symmetry of the cavity is broken and the SPP mode tends to be launched along the long axis of the cavity (which is $2\lambda_{SPP}$), Fig. 5(b). This effect becomes more evident at 60°, Fig. 5(c), where one can see a standing wave completely formed along the long length of the cavity. Therefore these modes are referred to here as longitudinal modes. Another consequence of tilting the cavity is that the field amplitude inside the cavity becomes considerably higher than that for a straight cavity. Particularly for $\theta = 60°$, Fig. 5(c), the field amplitude is about 29 times higher than that for $\theta = 0°$ (or about 7 times higher if both complex field amplitudes are considered in absolute value). This stronger field localization helps explain the improved quality factor observed for tilted cavities. Moreover, since the tilting angle changes the launching condition of the SPP mode, it is therefore expected that additional wavelengths resonate inside this cavity. This helps explain why additional resonant

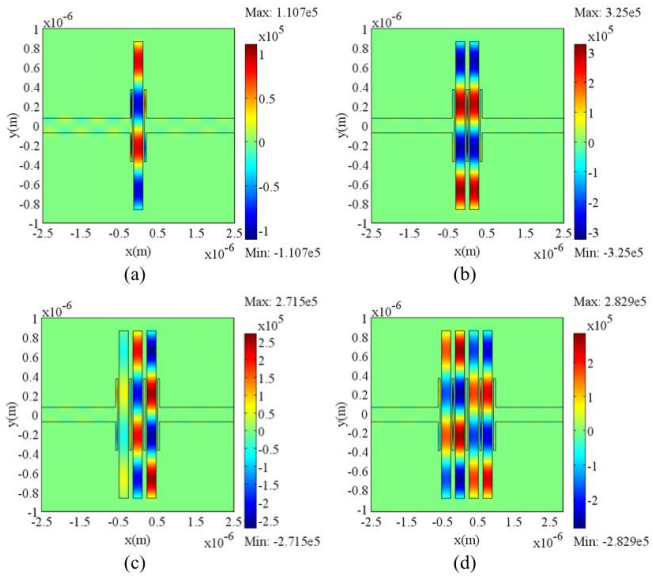

Fig. 6: Real part of the electric field distribution for the E_x component (V/m) for (a) single, (b) two, (c) three, and (d) four cascaded cavities. The tilting angle θ = 0°. The resonant wavelengths respective to (a)-(d) are 969.5 nm, 965.3 nm, 969.5 nm, and 965.1 nm.

peaks only appear for tilted cavities, as shown in Figs. 3(a)-(d). Observe, for example, the cases for $\theta = 30°$, 45°, and 60°. Besides the main peak at ≈ 971 nm (which is the desired peak), one can clearly see three additional peaks at approximately 570 nm, 650 nm, and 770 nm. Except for the peak around 650 nm (more pronounced for angles between 40° and 55°), all other peaks are approximately separated by 200 nm. In any case, the results also show that these "unwanted" resonances can be eliminated by a proper choice of angles, if desired.

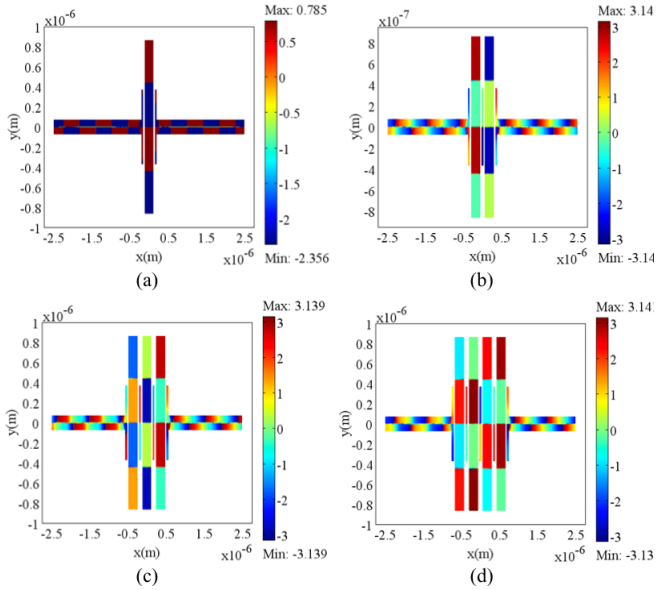

Fig. 7: Phase map distribution (rad) at resonance relative to the E_x component for (a) single, (b) two, (c) three, and (d) four cascaded cavities. The tilting angle θ = 0°.

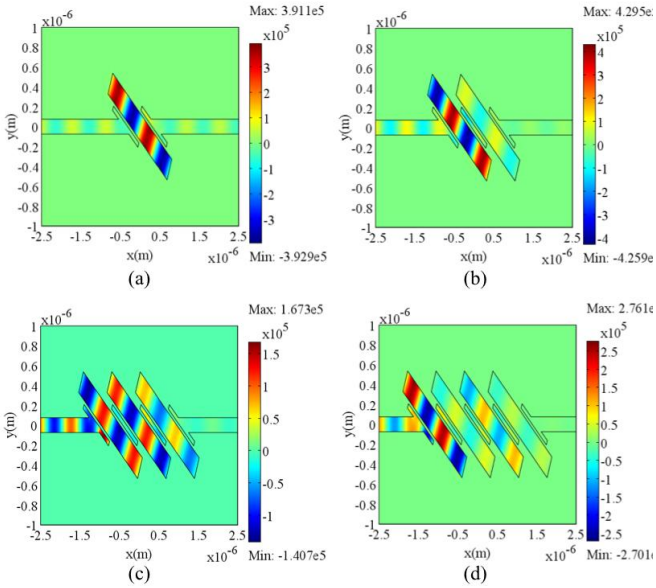

Fig. 8: Real part of the electric field distribution for the E_x component (V/m) for (a) single, (b) two, (c) three, and (d) four cascaded cavities. The tilting angle θ = 60°, and the resonant wavelengths respective to (a)-(d) are 969.5 nm, 969.5 nm, 967.3 nm, and 967.3 nm. The cavities appear distorted because the *x* and *y* axes are not in proportion.

Finally, we compare the electric field distribution (real part of the E_x component) and its corresponding phase map for the cascaded cavities at two distinct tilting angles, namely, $\theta = 0°$ (Figs. 6 and 7) and 60° (Figs. 8 and 9), taken at resonance. One can see from the field distributions in Figs. 6 and 8 that the height of the cavities are equal to $2\lambda_{SPP}$, while the total height of the stubs is approximately equal to λ_{SPP}. This stub/cavity height configuration is nearly optimum as it provides a better wave coupling to the central cavity(ies). As mentioned previously, the wave pattern inside the stub closely matches the wave cycle inside the cavity. Higher stubs improve wave coupling into and out of the cavity, therefore reducing transmission losses, but they do sacrifice the quality factor *Q*. The increased coupling into and out of the cavity reduces the energy stored inside the cavities, causing the quality factor *Q* to be reduced. The phase map distribution helps provide insight into the resonance condition for all SPP structures. The phase pattern shows that the phase is constant except at the nodal points where the signs change abruptly, which is the signature of a standing wave. Regarding the additional peaks at 570 nm, 650 nm, and 770 nm, their phase maps (even though not shown here) present precisely the same behavior. Therefore, we can clearly state that these extra wavelengths also resonate inside the cavities.

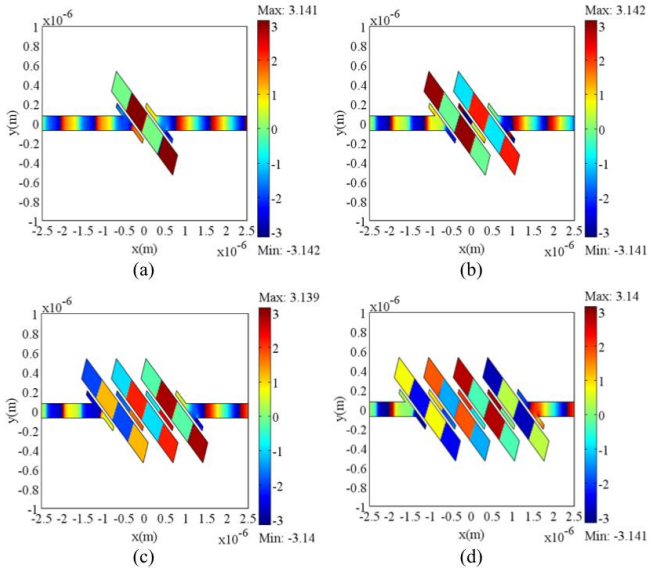

Fig. 9: Phase map distribution (rad) at resonance relative to the E_x component for (a) single, (b) two, (c) three, and (d) four cascaded cavities. The tilting angle $\theta = 60^o$. The cavities appear distorted because the *x* and *y* axes are not in proportion.

IV. Conclusion

We have proposed a novel design for metal-insulator-metal SPP-based structures aiming at wavelength filtering applications. The structure consisted of a subwavelength MIM waveguide with transversely arranged tilted cavity. We have carried out an analysis of pertinent geometrical parameters of the structure aiming at finding optimum configurations. Simulation results have shown that single and double cascaded cavities are a good compromise between wavelength selectivity and transmission losses. In addition, we have shown that the extra degree of freedom provided by the tilting of the cavity not only improved the quality factor of the structures, but also allowed for tuning multiple wavelengths. These additional resonant wavelengths, not observed for single and not tilted cavities, can clearly extend the range of applications for these structures.

Acknowledgment

This work has been carried out in the National Institute for Optics and Photonics (INOF) which has the financial support from FAPESP and CNPq.

References

[1] P.Berini, "Plasmon-polariton waves guided by thin lossy metal films of finite width: Bound modes of symmetric structures," *Phys. Rev. B*, vol. 61, no. 15, pp. 10484-10503, April 2000.

[2] B. Steinberger, A. Hohenau, H. Ditlbacher, A. L. Stepanov, A. Drezet, F. R. Aussenegg, A. Leitner, and J. R. Krenn, "Dielectric stripes on gold as surface plasmon waveguides," *Appl. Phys. Lett*., vol. 88, 094104, 2006.

[3] R. Charbonneau, P. Berini, E. Berolo and E. Lisicka-Shrzek, " Experimental observation of plasmon–polariton waves supported by a thin metal film of finite width," *Opt. Lett.*, vol. 25, no. 11, pp. 844-846, June 2000.

[4] A. Boltasseva, T. Nikolajsen, K. Leosson, K. Kjaer, M. S. Larsen, and S. I. Bozhevolnyi, " Integrated Optical Components Utilizing Long-Range Surface Plasmon Polaritons," *J. Lightw. Technol.*, vol. 23, no. 1, pp. 413-422, Jan. 2005.

[5] R. Charbonneau, C. Scales, I. Breukelaar, S. Fafard, N. Lahoud, G. Mattiussi, and P. Berini, " Passive Integrated Optics Elements Based on Long-Range Surface Plasmon Polaritons," *J. Lightw. Technol.*, vol. 24, no. 1, pp. 477-494, Jan. 2006.

[6] T. Holmgaard, Z. Chen, S. I. Bozhevolnyi, L. Markey, and A. Dereux, " Design and Characterization of Dielectric-Loaded Plasmonic Directional Couplers," *J. Lightw. Technol.*, vol. 27, no. 24, pp. 5521-5528, Dec. 2009.

[7] B. Steinberger, A. Hohenau, H. Ditlbacher, F. R. Aussenegg, A. Leitner, and J. R. Krenn, " Dielectric stripes on gold as surface plasmon waveguides: Bends and directional couplers," *Appl. Phys. Lett*., vol. 91, 081111, 2007.

[8] Y. Pennec, B. Djafari-Rouhani, A. Akjouj, J. O. Vasseur, L. Dobrzynski, J. P. Vilcot, M. Beaugeois, M. Bouazaoui, R. Fikri, and J. P. Vigneron, "Transmission filtering of a waveguide coupled to a stub microresonator," *Appl. Phys. Lett*., vol. 89, 101113, 2006.

[9] Y. Pennec, M. Beaugeois, B Djafari-Rouhani, A Akjouj, J. O. Vasseur, L. Dobrzynski, J.-P. Vilcot, M. Bouazaoui and J.-P. Vigneron, "Selective filtering of confined optical waves in a straight waveguide coupled to lateral stubs," *J. Opt. A: Pure Appl. Opt*., vol. 9, pp. S431–S436, 2007.

[10] Y. Pennec, M. Beaugeois, B. Djafari-Rouhani, R. Sainidou, A. Akjouj, J.O. Vasseur, L. Dobrzynski, E.H. El Boudouti, J.-P. Vilcot, M. Bouazaoui and J.-P. Vigneron, "Microstubs resonators integrated to bent Y-branch waveguide," *Photon. Nanostruct.: Fundam. Applic*., vol. 6, pp. 26–31, 2008.

[11] R. Zia, M. D. Selker, P. B. Catrysse, and M. L. Brongersma, " Geometries and materials for subwavelength surface plasmon modes," *J. Opt. Soc. Am. A*, vol. 21, no. 12, pp. 2442-2446, Dec. 2004.

[12] X.-S. Lin and X.-G. Huang, "Tooth-shaped plasmonic waveguide filters with nanometeric sizes," *Opt. Lett.*, vol. 33, no. 23, pp. 2874-2876 Dec. 2008.

[13] J. -Q. Liu, L.-L. Wang, M.-D. He, W.-Q. Huang, D. Wang, B. S. Zou, and S. Wen, "A wide bandgap plasmonic Bragg reflector," *Opt. Express*, vol. 16, no. 7, pp. 4888-4894, March 2008.

[14] J. Tao, X. G. Huang, X. Lin, Q. Zhang, and X. Jin, "A narrow-band subwavelength plasmonic waveguide filter with asymmetric multiple-teeth-shaped structure," *Opt. Express*, vol. 17, no. 16, pp. 13989–13994, Aug. 2009.

[15] X. Lin and X. Huang, " Numerical modeling of a teeth-shaped nanoplasmonic waveguide filter," *J. Opt. Soc. Am. B*, vol. 26, no. 7, pp. 1263-1268, July 2009.

[16] Y. Gong, L. Wang, X. Hu, X. Li, and X. Liu, "Broad-bandgap and low-sidelobe surface plasmon polariton reflector with Bragg-grating-based MIM waveguide," *Opt. Express*, vol. 17, no. 16, pp. 13727-13736, Aug. 2009.

[17] J. Tao, X. G. Huang, X. Lin, J. Chen, Q. Zhang, and X. Jin, "Systematical research on characteristics of double-sided teeth-shaped nanoplasmonic waveguide filters," *J. Opt. Soc. Am. B, vol.* 27, no. 2, pp. 323-327, Feb. 2010.

[18] A. Hosseini and Y. Massoud, "Nanoscale surface plasmon based resonator using rectangular geometry," *Appl. Phys. Lett.*, vol. 90, 181102, 2007.

[19] A. Noual, Y. Pennec, A. Akjouj, B. Djafari-Rouhani and L. Dobrzynski, "Nanoscale plasmon waveguide including cavity resonator," *J. Phys. Condens. Matter*, vol. 21, 375301, 2009.

[20] Q. Zhang, X.-G. Huang, X. S. Lin, J. Tao, and X.-P. Jin, "A subwavelength coupler-type MIM optical filter," *Opt. Express*, vol. 17, no. 9, pp. 7549-7554, April 2009.

[21] S. Xiao, L. Liu, and M. Qiu, "Resonator channel drop filters in a plasmon-polaritons metal," *Opt. Express*, vol. 14, no. 7, pp. 2932-2937, April 2006.

[22] L. O. Diniz, F. D. Nunes, E. Marega and B.-H. V. Borges, " A novel subwavelength plasmon polariton optical filter based on tilted coupled structures," *Proc. META'10 2nd International Conference on Metamaterials, Photonic Crystals and Plasmonics*, pp. 106-110, Cairo, Egypt, 2010.

[23] Johnson, P. B. and R. W. Christy, "Optical constants of the noble metals," *Phys. Rev. B*, vol. 6, no. 12, pp. 4370-4379, Dec. 1972.

[24] COMSOL Multiphysics, www.comsol.com.

[25] P. Berini, R. Charbonneau, N. Lahoud, and G. Mattiussi, "Characterization of long-range surface-plasmon-polariton waveguides," *J. Appl. Phys*, vol. 98, 043109, 2005.

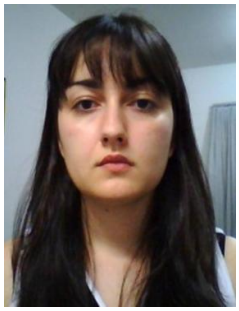

Lorena O. Diniz was born in Goiânia-GO, Brazil, in 1985. She received the degree in Electrical Engineering from University of São Paulo (USP), São Carlos-SP, Brazil, in 2007. She is currently working toward the M.Sc. degree in Electrical Engineering - Telecommunication at USP, São Carlos, Brazil. Her current research interests include modeling of optical devices based in Surface Plasmon Polariton (SPP) waveguides.

Frederico D. Nunes received the Ph.D. degree in Physics from Institute of Physics Gleb Wataghin-Unicamp, Campinas, São Paulo, in 1977. He became Professor at Unicamp in 1974 His work has covered semiconductor lasers. In 1980 he joined the Center of Research and Development of Telebras working with optoelectronic devices for telecommunication. In 1987 he was with Elebra Microelectronics heading optoelectronics department activities. Since 1997 he is with the Electronic and System Department in the Universidade Federal de Pernambuco. His current main interests are in nanophotonics, optics and photosyntesis. Dr. Nunes is member of the Optical Society of America, National Institute of Optics and Photonics (INOF) at USP-São Carlos.

Euclydes Marega, Jr. received the B.S. and Ph.D. degrees in Physics from University of Sao Paulo in 1988 and 1992 respectively. He is currently working as a Associate Professor at University of Sao Paulo. His current research interests are Nanostructure design and fabrication for photonics and electronics applications. He is also the coordinator of the NanofabLab at IFSC/USP.

John Weiner received his B.S. degree in Chemistry from the Pennsylvania State University in 1964 and his PhD degree in Chemical Physics from the University of Chicago in 1970. He was a Professor in the Chemistry Department of the University of Maryland from 1978 to 1996. In 1996 he moved to the Universite Paul Sabatier, in Toulouse, France from which he retired in 2007. In 2008 he was a visiting scholar at the IFSC in São Carlos and in 2009 he was appointed Visiting Fellow at the Center for Nanoscale Science and Technology (CNST) at the National Institute of Standards and Technology (NIST). His research interests have been in cold atom collisions interacting with light fields and the interaction of light and matter at the nanoscale.

Ben-Hur V. Borges received the Ph.D. degree in electrical engineering from Drexel University, Philadelphia, USA, in 1997. From 1997 to 1998 he was a post-doctoral researcher at the São Carlos School of Engineering of the University of São Paulo, in São Carlos, SP, Brazil. Since 2005, he is an Associate Professor at the University of São Paulo in São Carlos. His research interests are in metamaterials, plasmonics, modeling of devices for communications and sensing applications, and modeling of optical code multiple access networks.

Dr. Borges is a Member of the Optical Society of America (OSA) and IEEE.